J. Fluid Mech. (1987), *vol.* 176, *pp.* 237–252
Printed in Great Britain

Liquid impact on a bilinear elastic–plastic solid and its role in cavitation erosion

By M. McD. GRANT† AND P. A. LUSH
Thermo-Fluids Engineering Research Centre, The City University, London, EC1V 0HB, UK

(Received 4 July 1986)

The collapse of cavitation bubbles generates microjets which can cause local plastic deformation on neighbouring solid materials. This deformation takes the form of pitting which will eventually lead to large-scale material erosion. A model is presented which predicts the relative dimensions of the pits as a function of bubble collapse pressure, the shape of the microjet and the mechanical properties of the solid. The high pressures required to cause material deformation are generated by a water hammer mechanism and the solid is taken to have a simple bilinear elastic–plastic response. Measurements on pits produced by both flow and spark-generated cavitation are found to lie within the bounds predicted by the model. Both the measurements and the model suggest that there is a threshold microjet velocity below which no damage occurs, although such behaviour is masked, in practice, by statistical variations.

1. Introduction

It is well known that cavitation bubbles collapsing adjacent to a solid surface will do so asymmetrically directing a microjet towards the surface. A number of studies have produced photographic evidence of microjet formation; two of the most recent are Lauterborn (1979) and Kimoto, Tsuda & Hirose (1983). It is reasonable to suppose that the impact of the microjet on the solid surface has a major role in causing erosion. Although a substantial contribution to damage caused by the shock wave emanating from the collapse centre cannot be ruled out, attentuation by spherical spreading will considerably reduce the shock pressure at the solid surface.

Using a potential-flow analysis, Plesset & Chapman (1971) have considered the collapse of a vapour cavity adjacent to a solid surface and predicted microjet velocities in the region of 130 m/s for an external pressure equal to 0.1 MPa, i.e. atmospheric. To generate plastic flow in a material like aluminium, a flat punch must produce a surface pressure of about 400 MPa. For the stagnation pressure of the impacting microjet to reach such a value an external pressure of about 5 MPa would be required. Pressures as large as this will be rarely encountered in cavitating fluid systems and even higher pressures would be required for harder materials. If it is assumed that the microjet generates a water hammer pressure, then an external pressure of about 0.4 MPa is required for plastic flow. Such pressures are commonplace in cavitating components, so it can be deduced that the damage mechanism is dependent upon liquid compressibility effects.

A substantial body of literature has arisen regarding the generation of water

† Present address: Atkins R & D, Epsom, Surrey, UK.

hammer pressures during liquid–solid impact. Those aspects which are relevant to cavitation erosion are reviewed below.

The impact of a cylindrical liquid mass on a rigid solid has been considered by Glenn (1974), who demonstrated that impact pressures are considerably in excess of those calculated using simple linear theory. Bowden & Field (1964) were probably the first to postulate the mechanism whereby a curved drop will generate water hammer pressures as long as conditions at the contact point are supersonic, allowing an attached shock to form; Brunton & Rochester (1979) have shown photographic evidence of such shock waves. There is a critical velocity for the contact point below which the shock cannot remain attached; on shock detachment the liquid behind the shock is free to flow outwards, a phenomenon known as jetting, and the pressure drops to the stagnation value. Heymann (1969) solved the shock equations for two-dimensional impact of a wedge-shaped mass on a rigid surface. He found that, at the critical velocity required for shock detachment, pressures of up to $3\rho_0 c_0 v$ could be generated (v is impact velocity, ρ_0 and c_0 are ambient values of ρ and c). For a rounded drop the velocity of the contact point is initially infinite, but as the impact proceeds the contact velocity decreases until shock detachment and then jetting occurs. Thus the highest pressure will be generated at the perimeter of the impact. Rochester & Brunton (1979) have confirmed this experimentally, finding that the pressure is about $\rho_0 c_0 v$ at the centre of the impact, rising to about $2.5\rho_0 c_0 v$ at the perimeter. Heymann's analysis has since been reworked by Field, Lesser & Davies (1979) using a more accurate equation of state for water; however the solution only differs in detail. The above analysis applied to a curved liquid surface can give only the pressure directly behind the shock. Lesser (1981) has developed a geometrical acoustics technique which allows the pressure at any point behind the shock to be calculated and this technique can also be employed to solve the problem in three dimensions. It is demonstrated that the three-dimensional pressure directly behind the shock is less than the two-dimensional result by a factor of between 0.8 and 1.0, the exact value depending upon the time after impact. In the same paper, Lesser considers the effect of material elasticity and finds that it delays the onset of jetting and reduces the pressure generated. Field, Lesser & Dear (1985) have measured very high fluid velocities associated with jetting. It seems likely that jetting may contribute to the erosion process in some cases.

The motivation of much of the work noted above has been the need to understand the mechanism of damage and erosion, which often accompanies liquid impact. In order to do this, the behaviour of the solid must be considered together with the fluid behaviour. As already mentioned, Lesser (1981) has done this for the impact of droplets on a purely elastic material. Recently one of the present authors (Lush 1979, 1983) has considered the case of the impact of both plane-ended and wedge-shaped liquid jets on a rigid–perfectly plastic solid. The nominal surface slope (i.e. maximum depth divided by radius) of the resulting pit was calculated in terms of the material hardness and the impact velocity. In this paper, we have extended the original analysis to deal with the more realistic case of impact on a bilinear elastic–plastic solid (see figure 1); the cases of rigid–plastic and elastic–perfectly plastic solids are also considered in order to illustrate individually the effects of elasticity and work hardening. The impact of plane-ended and wedge-shaped jets is considered separately; although the former is not likely to be realistic, the analysis is somewhat simpler and serves to illustrate the salient features of the liquid impact.

By considering impact on plastic materials, the theoretical predictions can be readily compared with experimental data; this has been done for cavitation pits

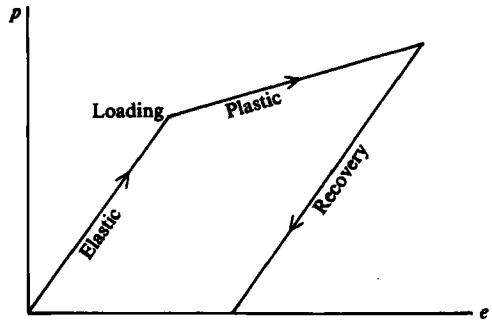

FIGURE 1. Loading–unloading response of a bilinear elastic–plastic material.

produced in 99% pure aluminium by both hydrodynamic cavitation and spark-induced bubbles, and for various aluminium alloys subjected to spark-induced bubbles.

2. The impact of a liquid mass on a bilinear elastic–plastic solid

2.1. *Plane-ended jet*

When a plane-ended jet, initially travelling with velocity v, impacts a solid surface, the liquid at the centre of the jet is unable to flow outwards and a shock wave is propagated away from the surface. There is a pressure, p, of water hammer magnitude behind the shock wave. If the solid is non-rigid then it will be deformed with a velocity, u, equal to the fluid velocity behind the shock wave. The liquid at the edge of the jet is at ambient pressure and therefore free to flow outwards. A release wave is propagated inwards and, as it passes, the pressure drops from the water hammer value to a value between the ambient and stagnation pressure.

The relationships between p, v and u are obtained by applying the continuity and momentum equations across the shock and defining an equation of state for the liquid, in this case water, as follows:

$$\text{Continuity:} \qquad \rho_0(v+c) = \rho(u+c), \tag{1}$$

$$\text{Momentum:} \qquad p-p_0 = \rho_0(v+c)\,(v-u), \tag{2}$$

$$\text{Equation of state:} \qquad \frac{p+B}{p_0+B} = \left(\frac{\rho}{\rho_0}\right)^n, \tag{3}$$

where ρ and ρ_0 are the liquid densities behind and in front of the shock respectively. The ambient pressure p_0 is generally much lower than p and is henceforth ignored. B and n are constants taken to be 300 MPa and 7 respectively. The shock velocity is denoted by c and if the impact velocity were low the shock velocity could be taken as the sound speed; in this case (3) would be unnecessary.

As they stand, equations (1)–(3) are not sufficient to solve for p and u in terms of v. However, as the relationship between p and u is governed by the response of the solid, the equations can be solved if the stress–strain behaviour of the solid is known. The compressive stress–strain behaviour can be idealized by considering rigid or elastic responses, which have been commonly used for liquid drop impact analyses where failure usually occurs by brittle fracture. In attempting to model damage on aluminium we are more interested in plastic deformation, which can be idealized by considering rigid or elastic responses in combination with perfectly plastic, i.e.

constant yield stress, or plastic, i.e. work-hardening, responses. The most useful combination is probably the bilinear elastic–plastic stress–strain characteristic which incorporates both elastic and work hardening behaviour (see figure 1).

The pressure behind the shock, p_Y, which is required to initiate plastic deformation is taken to be three times the uniaxial yield stress of the material. This is the pressure that a flat punch or ball indenter must generate to establish full-scale plastic flow (see Tabor 1951). For 99% pure aluminium (S1C) as used in the present work, $3Y$ has been measured using a Vickers Diamond Pyramid indenter and found to be 400 MPa. The ratio of the elastic and plastic moduli is given by Jauol (1964) as 100 for 99.9% pure aluminium in tension. A similar figure is found for the compressional tests conducted by Penny (1981).

When the jet impacts the surface an elastic wave will propagate into the solid and, if the jet has sufficient velocity to generate a pressure p greater than p_Y, a plastic wave will also propagate behind the elastic wave. The wave speeds are denoted by c_e for the elastic and c_p for the plastic wave speed, which is constant as a result of the assumed bilinear response. As the ratio of moduli is 100 then c_e/c_p is 10 and $c_p = 630$ m/s since $c_e = 6300$ m/s for aluminium. Near the centre of the impact, the elastic and plastic wavefronts will be approximately plane and propagate in the direction normal to the solid surface. Applying the momentum equation across the elastic and plastic fronts, assuming that the wave speeds are much larger than the particle velocities in the solid, yields

$$p_Y = \rho_s c_e u_Y, \tag{4}$$

for the elastic wave front, and

$$p - p_Y = \rho_s c_p (u - u_Y), \tag{5}$$

for the plastic wave front, where u and u_Y are the particle velocities behind the plastic and elastic wave fronts respectively and ρ_s is the density of the solid. Eliminating u_Y gives:

$$u = \frac{p_Y}{\rho_s c_e} + \frac{p - p_Y}{\rho_s c_p}, \tag{6}$$

and combining (6) with the liquid shock relationships allows p and u to be calculated separately for values of v.

Once the release wave reaches the centre of the jet, the solid will no longer be stressed and a release wave will propagate into the solid. The release wave will travel at c_e and all plastic deformation will cease when it overhauls the plastic wave.

Once the solid is no longer stressed, that proportion of the deformation which is elastic (as opposed to plastic) will recover; see figure 1. Prior to unloading, the total compressive strain, e, behind the plastic wave front is given by

$$e = \frac{u_Y}{c_e} + \frac{u - u_Y}{c_p}, \tag{7}$$

and this may be written in terms of compressive stress, using (4) and (5), as follows:

$$e = \frac{p_Y}{\rho_s c_e^2} + \frac{p - p_Y}{\rho_s c_p^2}. \tag{8}$$

On unloading, the compressive strain recovered will be $p/\rho_s c_e^2$, and the residual, or permanent, plastic strain e_p can be obtained by subtracting the recovered strain from the total strain to give

$$e_p = \frac{(p - p_Y)}{\rho_s c_p^2}\left(1 - \frac{c_p^2}{c_e^2}\right). \tag{9}$$

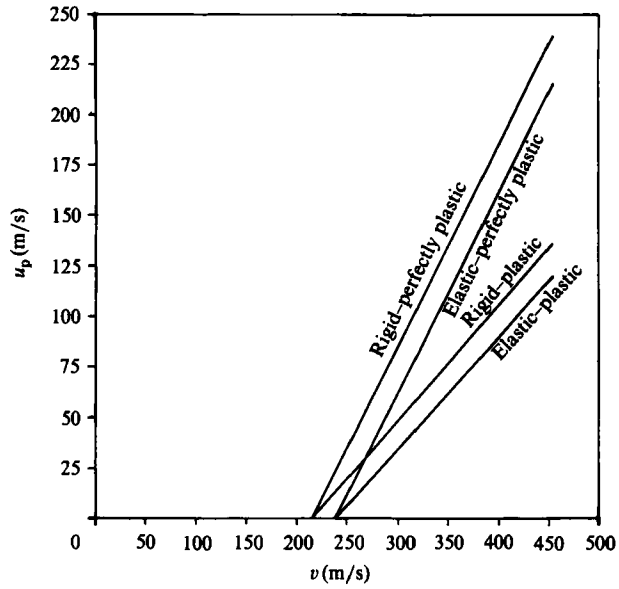

FIGURE 2. Plastic deformation velocity (u_p) versus impact velocity (v) for plane-ended jet on various plastic solids with $p_Y = 400$ MPa and full elastic recovery.

The effective velocity of plastic deformation u_p giving rise to this plastic strain will be $c_p e_p$, and with the aid of (6) this may be written as

$$u_p = \left(u - \frac{p_Y}{\rho_s c_e}\right)\left(1 - \frac{c_p^2}{c_e^2}\right). \tag{10}$$

Since c_p^2/c_e^2 is 0.01 for aluminium, the major proportion of the recovery is that associated with the elastic wave.

If the material is taken as rigid–plastic (i.e. $c_e \to \infty$) then there will be no recovery and u_p is simply equal to u. In the elastic–perfectly plastic case, the plastic deformation velocity is determined from (10) on putting $c_p = 0$.

For a given set of material and liquid constants and a given impact velocity, v, the equations (1)–(3) and (6) can be solved for p and u. The resulting value of u is then used in (10) to obtain the plastic deformation velocity which is required to calculate the permanent surface indentation. The relationship between u and v has been obtained using the constants appropriate to water and aluminium and is shown in figure 2. Included for comparison are the three other, simpler plastic materials, discussed earlier. In each case, it is seen that no deformation occurs until a threshold impact velocity is reached, corresponding to the impact velocity required to generate a pressure of p_Y. The effect of including elasticity in the material response is to raise the threshold impact velocity by about 10%; the inclusion of work hardening does not alter the threshold impact velocity but it does reduce the deformation velocity at impact velocities above the threshold.

2.2. *Wedge-shaped jet*

The impact of a two-dimensional wedge-shaped jet on a solid surface is shown in figure 3(*a*). If the contact point has sufficient lateral velocity then a shock, attached to the contact point, will form. The exact conditions which govern shock formation are

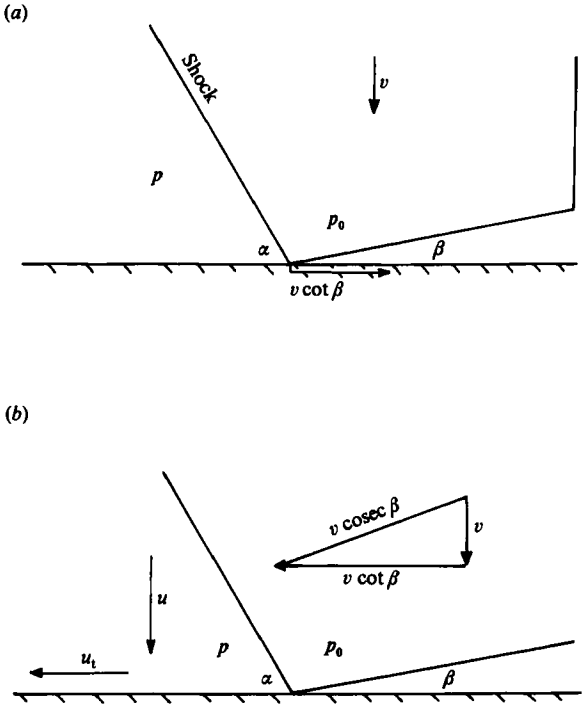

FIGURE 3(*a*) Wedge-shaped jet impact. (*b*) Wedge-shaped impact with stationary contact point.

complex and will be discussed later. Conditions behind the shock are best analysed by considering the contact point to be stationary as in figure 3(*b*). This is achieved by superimposing a lateral velocity equivalent to that of the contact point and assuming that the material immediately below the contact point does not deform. The velocity is resolved into components normal and parallel to the shock. The parallel component is unaffected by the shock and the transition of the normal component through the shock is governed by the equations of momentum, continuity and state as in (1), (2) and (3). Having obtained the velocity components downstream of the shock, these are resolved into components normal and parallel to the undeformed surface and the normal velocity is taken as the deformation velocity, u, at the centre of the impact zone. Lush (1983) has performed this analysis and gives the normal velocity, u, as

$$u = v \operatorname{cosec}\beta \sin(\alpha+\beta)\cos\alpha\left[\left(1+\frac{p}{B}\right)^{-1/n} - \frac{\tan\alpha}{\tan(\alpha+\beta)}\right], \tag{11}$$

the velocity transverse to the surface, u_t, as

$$u_t = v \operatorname{cosec}\beta \sin(\alpha+\beta)\sin\alpha\left[\left(1+\frac{p}{B}\right)^{-1/n} + \frac{1}{\tan\alpha\tan(\alpha+\beta)}\right], \tag{12}$$

and the pressure behind the shock, p, as

$$p = \rho_0 v^2 \operatorname{cosec}^2\beta \sin^2(\alpha+\beta)\left[1-\left(1+\frac{p}{B}\right)^{-1/n}\right]. \tag{13}$$

As in the case of the plane-ended jet, these equations can be solved if the response of the solid is known.

The impact of a wedge-shaped jet on an elastic–plastic solid is now considered. The treatment of the solid is the same as for the plane-ended jet but with only the material at the centre of the impact zone being considered and with effectively plane elastic and plastic waves being propagated into the solid. Thus the solid response is given by (6) and the material parameters are again taken as for aluminium. Equations (6), (11) and (13) cannot be solved directly, and a simple iterative technique has been employed. Values of β and α are fixed and p is initially set at p_Y, allowing an estimate of u to be obtained from the liquid shock relations (11) and (13). This value of u is used in the material response equation (6) to obtain a new estimate for p, which becomes the starting value in the next iterative step. The solution is considered complete when the difference in subsequent values of p is less than 100 Pa, corresponding to a fractional error of, at most, 2.5×10^{-7} in p.

For given values of v and β, two values of p may exist, representing the weak and strong shock solutions. Only one solution exists for $\beta = 0°$, the plane-ended case, and this is consistent with the weak shock solution as β approaches zero. Therefore the weak shock solution is taken as the one which will occur in practice. As v is lowered for a given β, a point is reached where the weak and strong shocks are coincident and no solution is available if v is lowered further. In reality the shock cannot remain attached to the contact point if v were to be lowered further. If this occurs the liquid is free to flow outwards and the pressure will not rise above the stagnation value.

An additional complication in this analysis is that as v is lowered the fluid velocity behind the shock will become subsonic and disturbances will be able to propagate towards the contact point. The point at which this occurs is, in general, obtained by equating the fluid velocity to the local sonic velocity c, given by

$$c = c_0 \left(1 + \frac{p}{B}\right)^{(n-1)/2n}. \tag{14}$$

Exactly what happens as v is reduced below the sonic point towards the detachment condition is not clear. However, it seems reasonable to suppose that the shock will remain attached, although it may become curved. If it does curve, the solution for a straight shock will only be strictly applicable in the immediate vicinity of the contact point. This is an area requiring further work and, at this point, it is simply assumed that no significant errors are introduced into the analysis.

The material is assumed to undergo full elastic recovery after loading has ceased, using (10). The relationship between u_p and v for various values of β is shown in figure 4. The picture is broadly the same as for the rigid–perfectly plastic case, with the detachment points lying approximately on a straight line. The detachment loci for all four plastic cases are shown together in figure 5. It is seen that the effect of including elasticity is to increase the threshold value of v. The inclusion of work hardening both decreases the gradient and increases the threshold value of v.

Considering the material as being purely elastic gives a relationship between p and v which is qualitatively the same as for the rigid case. The purely elastic detachment locus, with ρ_s and c_e as for aluminium, is given by

$$p = 2.47 \rho_0 c_0 v. \tag{15}$$

Comparison with the corresponding rigid case shows that, for a given velocity, the pressure generated is about 15 % less if elasticity is included. Additionally, for a given impact velocity it is found that the inclusion of elasticity in the model increases the wedge angle at which shock detachment occurs, in agreement with the results of Field Lesser & Dear (1985). To generate the yield pressure of 400 MPa, a velocity of 112 m/s

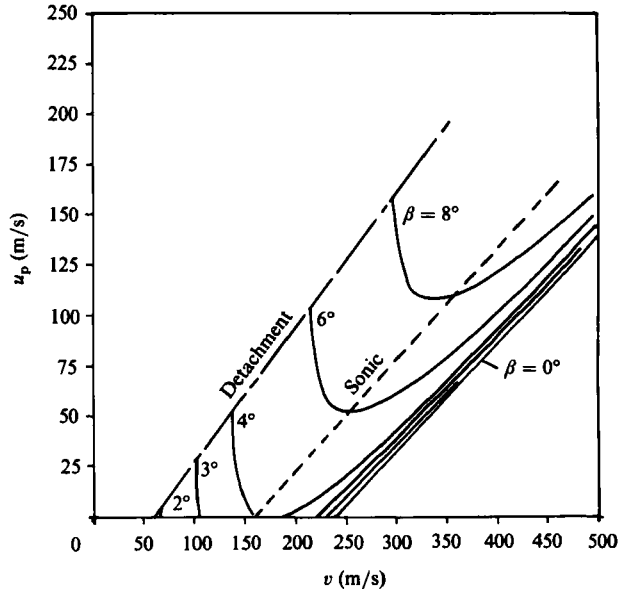

FIGURE 4. Plastic deformation velocity (u_p) versus impact velocity (v) for wedge-shaped jet with various wedge angles on an elastic–plastic solid with $p_Y = 400$ MPa and full recovery.

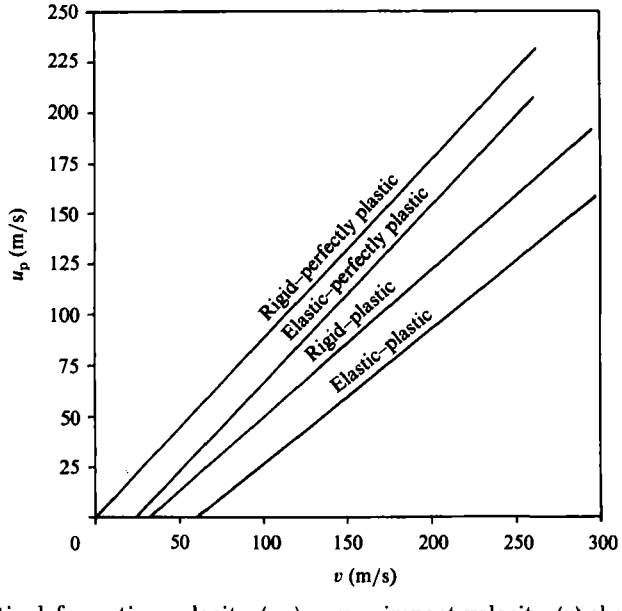

FIGURE 5. Plastic deformation velocity (u_p) versus impact velocity (v) showing only detachment loci for four plastic materials with $p_Y = 400$ MPa and full elastic recovery where appropriate.

is required. Referring back to the elastic–plastic case in figure 4, it is seen that the detachment locus predicts a threshold impact velocity of 60 m/s. The reason for this discrepancy is not known, but it may be related to the sudden change in boundary conditions as the material crosses the elastic–plastic discontinuity.

Assuming that deformation at the centre of the jet begins immediately upon impact and continues until the release wave reaches the centre of the jet, the time t over which

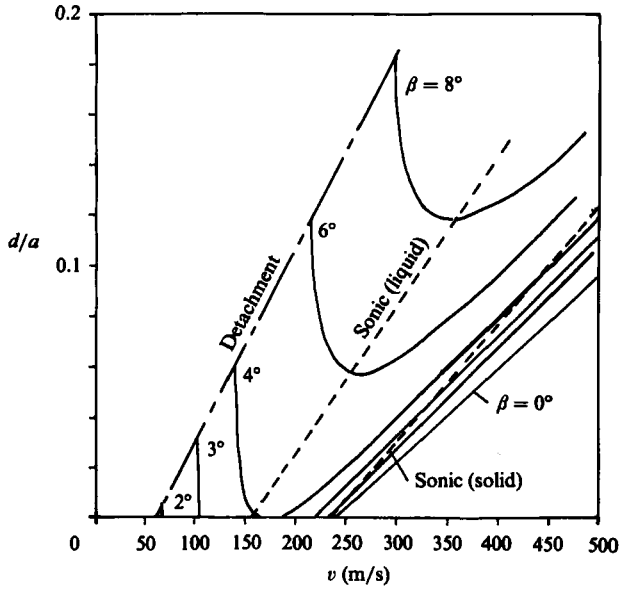

FIGURE 6. Pit slope (d/a) versus impact velocity (v) for wedge-shaped jet with various wedge angles on an elastic–plastic solid with $p_Y = 400$ MPa and full recovery.

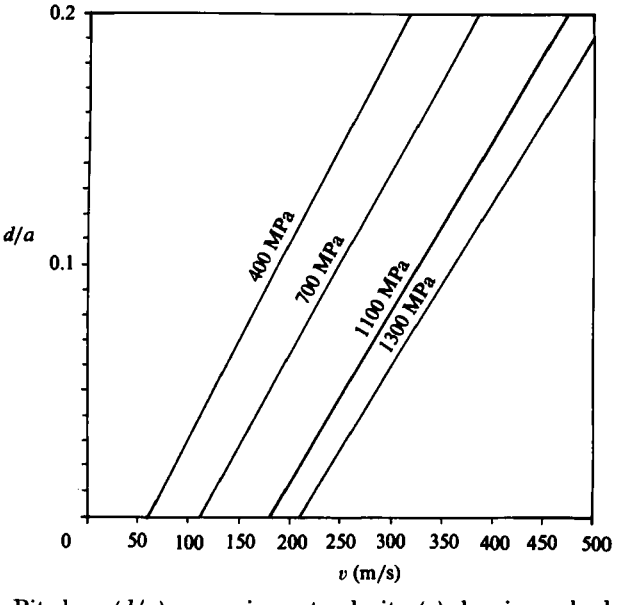

FIGURE 7. Pit slope (d/a) versus impact velocity (v) showing only detachment loci for elastic–plastic material with full recovery for various p_Y.

deformation occurs is given by the sum of the time delay between the impact of the tip and the outer radius of the jet and the time for the release wave to travel inwards to the centre, i.e. $a/(v\cot\beta)+a/c_0$, where a is jet radius . The depth d of the pit at the centre of the jet can be calculated by multiplying by u_p, and hence the nominal pit slope d/a is given by

$$\frac{d}{a} = \frac{u_p}{c_0}\left[\frac{c_0\tan\beta}{v}+1\right]. \tag{16}$$

The variation of d/a with v for various values of β is shown for the elastic–plastic material in figure 6. The detachment points again lie approximately on a straight line. Additionally, for a given impact velocity, it is found that by including plasticity the wedge angle for shock detachment is increased in a way similar to that found by including elasticity.

The effect on the detachment locus of varying p_Y is shown in figure 7. The values of ρ_s, c_e and c_p are unchanged, this being consistent with examining a variety of aluminium alloys. It is seen that increasing p_Y tends to decrease slightly the slope of the detachment locus and increase the threshold velocity.

In the analysis presented here only plane waves propagated from the impact centre have been considered; however the overall wave propagation picture is considerably more complicated. For the range of impact velocities considered here the elastic wave speed will, usually, be larger than the contact edge speed; the limit for the condition is shown in figure 6. The plastic wave speed at 10% of the elastic wave speed will always be slower than that contact speed if a shock is formed in the liquid. In addition to the elastic compressional wave, an elastic shear wave will be propagated at a velocity of about $\frac{1}{2}c_e$. Unless exceptionally high impact velocities in combination with small wedge angles are encountered, the elastic waves will always be well ahead of the contact point, (see Lesser & Field 1983).

It is clear that the interaction of stress waves in the vicinity of the contact edge is complicated. However, to calculate maximum penetration, i.e. at the centre of the impact, there is no need to consider the situation away from the centre.

3. Consideration of pits produced by cavitation

3.1. *Measurements of average surface slope*

The average surface slope (S_A) of aluminium during the early stages of cavitation damage has been measured using a surface profilometer (Rank Taylor Hobson Talysurf 5). The average surface slope is defined as follows:

$$S_A = \frac{1}{l}\int_0^l \left|\frac{dy}{dx}\right| dx, \tag{17}$$

where y is the surface displacement at position x and l is the total length of the sample. The particular profilometer used gives a direct reading of roughness average only; thus to allow S_A to be calculated the surface profile signal is transferred to a Honeywell 66/60 mainframe computer for processing. Further details regarding data acquisition and processing are given in Grant (1984).

A typical variation of S_A with time is shown in figure 8. It is seen that the relationship is linear, intercepting the positive S_A axis at zero time. It is assumed that the value of S_A at zero time $S_A(t_0)$ is characteristic of pitting before individual pits have been deepened by subsequent impacts. Filtering was found to be very important in achieving consistent results for $S_A(t_0)$. The optimum wavelength range was found to be 0.1 mm–0.55 mm, and this was therefore employed here. The profilometer traces a straight line which crosses the projected surface area of the pits at any random position. Assuming the pits to be circular, contiguous and uniform in dimensions allows $S_A(t_0)$ to be related to the nominal pit slope d/a, as follows:

$$\frac{d}{a} = \frac{2}{\pi - 2} S_A(t_0). \tag{18}$$

The variation of d/a with velocity is shown in figure 9. It is seen that the velocity

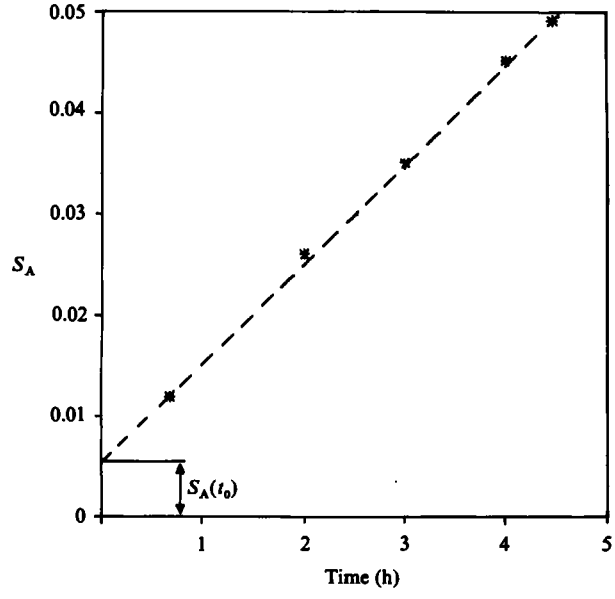

FIGURE 8. Average surface slope (S_A) versus time showing zero time intercept; $U = 24$ m/s, for symmetrical wedge.

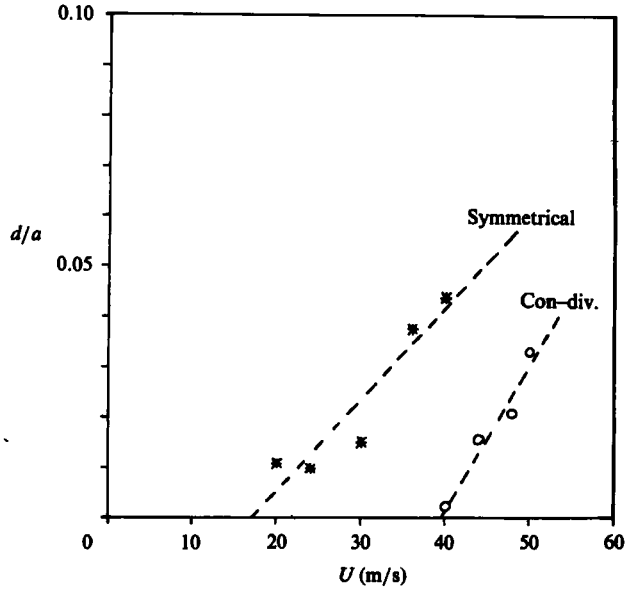

FIGURE 9. Measured slope (d/a) versus throat velocity (U) for con–div and symmetrical wedges.

data can be fitted by a linear equation, which predicts an apparent threshold flow velocity below which no damage occurs.

Using regression analysis, the following equations were fitted to the data, with the velocity U in m/s:

$$\text{Symmetrical wedge inducer:}\quad d/a = 0.001\,83(U-17.0), \tag{19}$$

$$\text{Con–Div wedge inducer:}\quad d/a = 0.002\,82(U-39.4). \tag{20}$$

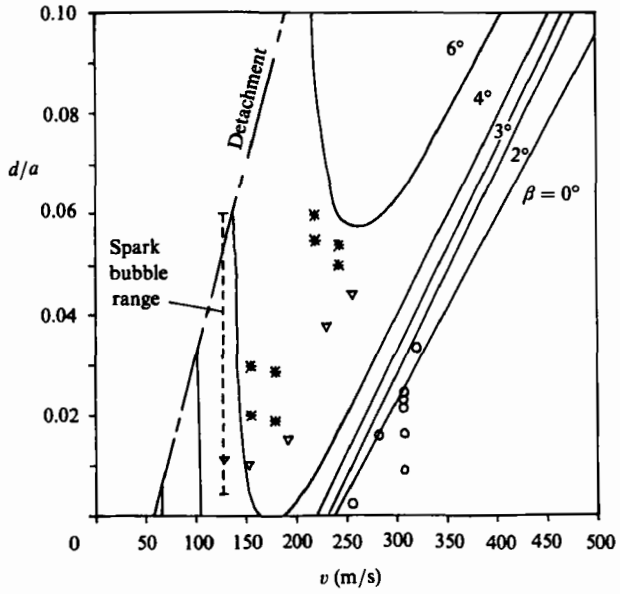

FIGURE 10. Comparison of experimental and theoretical values of slope (d/a) and impact velocity (v), for the following data: *, Lush (1979); ○, con–div wedge; ▽, symmetrical wedge.

Lush (1979) has conducted a similar investigation on aluminium using the con–div wedge in a slightly larger working section. Measuring the pit slope manually from the profilometer pen trace, he found

$$d/a = 0.0025(U - 14.9). \tag{21}$$

In principle there should be no problem in comparing results between the different sizes of working section, as d/a is a non-dimensional parameter. The slopes of the three equations (19), (20) and (21) are in reasonable agreement. The threshold velocities for the symmetrical wedge data and the con–div wedge data of Lush (1979) are also in reasonable agreement. The only discrepancy is the threshold velocity for the present con–div wedge data given by (20).

According to Plesset & Chapman (1971), the microjet velocity, v, is related to the pressure tending to collapse the cavity as follows:

$$v = 12.8\left(\frac{p_\infty - p_v}{\rho}\right)^{\frac{1}{2}}. \tag{22}$$

For the present flow configuration, the pressure external to the collapsing cavities is essentially given by the Borda–Carnot recovery pressure, which for a 50 % blockage, as here, is given by $0.5(\frac{1}{2}\rho U^2)$, where U is throat velocity. Hence it may be deduced that the microjet velocity is related directly to throat velocity by

$$v = 6.4U. \tag{23}$$

It is important to note that (23) is approximately independent of cavitation number when the cavitation number is small.

3.2. *Comparison with theory*

It has been shown how the maximum slope of a typical cavitation pit can be obtained from profilometer measurements and that the microjet velocity can be deduced from the throat velocity. We can therefore compare these measurements with the theory derived in §2. This is done in figure 10; also included are the results presented by Lush (1979) for the con–div wedge inducer. In general the results lie within the region bounded by the detachment locus and the line for plane-ended impact, except for some of the present con–div wedge data. Fitting a linear least-squares equation to the three sets of data yields

$$\text{Symmetrical wedge:} \quad d/a = 0.000285(v-109), \tag{24}$$

$$\text{Con–div wedge:} \quad d/a = 0.000366(v-248), \tag{25}$$

$$\text{Con–div wedge (Lush 1979):} \quad d/a = 0.000393(v-97.7). \tag{26}$$

It should be noted that these equations are not exactly related to (19)–(21), using (23), because a number of additional points have been included in the regression analysis. These points arise from tests where velocity was held constant while the cavitation number was varied.

Each equation predicts a threshold impact velocity, v_0, below which no damage will occur. The three data groups have similar gradients and lie approximately parallel to both the detachment locus and $\beta = 0°$ line. The value of v_0 is about 100 m/s for (24) and (26). It is, however, much higher for (25), and it may be that in this case the range of U and hence v which was considered was not wide enough to obtain an accurate result. A further possibility is that there may be a scale effect operating.

Lush, Wood and Carpanini (1983) have measured the nominal slope of pits produced on aluminium by the collapse of a bubble initially formed by sudden electrical discharge. The bubbles collapse at atmospheric pressure, and therefore from (22) the jet velocity is 128 m/s. The range of slope obtained is shown in figure 10 and it is seen that the upper limit corresponds fairly closely to the detachment locus.

Further work using the same test facility has been performed by Radish (1984), who tested three aluminium alloys in addition to pure aluminium. The values of p_Y were 400 MPa, 700 MPa, 1100 MPa and 1300 MPa, and these figures were used in the model predictions of detachment loci shown in figure 7. Since the microjet impact velocity is 128 m/s, it is seen from figure 7 that pitting would only be expected on pure aluminium (400 MPa) and the softest alloy (700 MPa). However, Radish found that all four materials displayed some pitting, with the average slope decreasing from 0.035 for pure aluminium (400 MPa) to 0.027 for the hardest alloy (1300 MPa). The probability of an individual collapse generating a pit was also found to decrease, ranging from 0.9 for pure aluminium to 0.3 for the hardest alloy. It is clear that a statistical effect is operating; bubbles collapsing at a particular external pressure will generate microjets having a range of values of v and β. Thus, for a given material, it would be expected that an increase in collapse pressure would increase the probability of a particular bubble causing a pit and also increase the nominal pit slope.

4. Discussion

One difficulty with the model which has not been fully resolved is the question of elastic recovery. Were the impact truly one-dimensional then full elastic recovery would occur after unloading. However, as the impact occurs on the surface of a half space it seems likely that any plastic deformation will tend to trap some underlying elastic deformation. The amount of elastic recovery will probably depend on the degree of plastic deformation. For small amounts of plastic deformation elastic recovery is likely to be almost complete, whereas, on the other hand, large-scale plastic flow will severely limit the amount of recovery. The elastic deformation predicted by the model has been considered to recover fully. Whilst this assumption is not completely valid, it is argued that full recovery is the most realistic, bearing in mind the shallow nature of the cavitation pits.

The detachment locus represents the theoretical maximum limit of deformation at a particular impact velocity. For the elastic–plastic material with a yield pressure of 400 MPa, the threshold impact velocity, below which no damage occurs, is predicted to be 60 m/s. The detachment locus for a purely elastic material suggests that impact below 112 m/s will not generate pressures in excess of 400 MPa. If the yield pressure is not reached then no deformation can occur, indicating that there is an anomaly between the elastic–plastic and the elastic cases. The threshold velocity of 112 m/s predicted from the elastic case agrees reasonably well with two of the threshold velocities predicted by the pit measurements, i.e. 98 m/s and 109 m/s in (24) and (26) respectively. As the jet impact velocity and the flow velocity are simply related by a multiplication factor, it might seem reasonable to suppose that there is a threshold flow velocity, below which no damage occurs. Mass loss measurements suggest that no such velocity exists with the mass loss rate varying simply as some power of the flow velocity. The two observations are not incompatible if it is postulated that there is, as seems likely, a stochastic element operating. In this case bubbles collapsing in conditions where the mean microjet velocity is below the threshold will have a low probability of causing damage. Bubbles collapsing with mean microjet velocities which are above the threshold will have a much higher probability of causing damage. It is not difficult to imagine how such behaviour could manifest itself as a power law relationship over the relatively narrow range of flow velocities typically considered in cavitation studies.

The compressive stress–strain relationship used here to describe the deformation behaviour of the solid assumes that indentation proceeds as simple uniaxial compression but with a threefold increase in yield pressure. However, it is known that during indentation, plastic deformation will begin at $1.1Y$ (Tabor 1951), the yield pressure only rising to $3Y$ once full-scale plastic flow has developed. A more realistic stress–strain relation may be represented by a continuous change of slope between the linear elastic and linear plastic regions. It would appear that the simplistic pressure-deformation behaviour used in the model is acceptable for large deformations but is perhaps less applicable in the early stages of plastic flow, where the transition from the elastic to the plastic regimes is gradual rather than abrupt, as in the bilinear model. This factor will tend to accentuate the difference between the idealized and actual behaviour. That some deformation is possible at pressures considerably less than $3Y$ is probably necessary to explain the results of Radish (1984), who found that jets which had insufficient velocity to generate pressures of $3Y$ would sometimes produce pits. A model utilizing a more complex form of

stress–strain behaviour than the bilinear case would probably require a finite element approach as utilized by Pederson, Pederson & Hansson (1983).

It has been shown that the wedge angle has a significant effect on the damage process. The numerical studies of Plesset & Chapman show β to be about 36° for a cavitation bubble microjet. This angle is far too large to allow an attached shock to form at the velocities considered here. However, if the jet angle is subject to some statistical variation then some jets will have sufficiently low values of β for shocks to form. No pit measurements from hydrodynamic cavitation were recorded near the detachment locus. However, this is hardly surprising, as a jet with a given wedge angle will only approach detachment if it has a velocity within a very narrow range.

Given the complexity of the liquid impact problem, the analysis presented here is necessarily somewhat idealized. For example, no attempt has been made to include the effects of jetting, which may be a significant factor during erosion in producing the removal of material in the form of asperities. Although the analysis deals only with pitting at the early stages of damage, when jetting is not likely to be important, a full understanding of the damage process must take into account the effect of jetting. A further simplification in the analysis is the assumption that bubble collapse is produced by the local static pressure. It is possible that shock waves from the collapse of adjacent bubbles may increase the severity of collapse and introduce a random element in the microjet velocity, which generates the stochastic behaviour discussed earlier. Further studies of individual bubble collapse may help resolve this matter.

5. Conclusions

A model predicting the surface slope of a cavitation pit produced in a bilinear elastic–plastic medium by an impacting microjet has been presented. The model predicts significant variations in behaviour, depending on whether the microjet is plane-ended or wedge-shaped. For the plane-ended jet there is a threshold velocity, which depends on plastic flow stress, below which no deformation occurs. Above this threshold the increase in deformation is linear with impact velocity.

For the wedge-shaped impacting jet, the deformation for a particular impact velocity depends on the wedge angle and lies between two limits. The lower limit coincides with the plane-ended jet above the original threshold velocity and with zero deformation below this velocity. The upper limit is given by the locus of shock detachment, which is approximately linear in all cases. This locus can also be used to define a new threshold velocity below which no deformation can occur. The threshold velocity increases with yield stress and the gradient of the detachment locus slightly decreases.

It is clear that the wedge-shaped jet generates deformation considerably more severe than the plane-ended jet; including the effects of elasticity and work hardening generally reduces the deformation and increases threshold velocity.

The predictions of surface slope, which should in principle be independent of size, have been compared with measurements and an encouraging agreement has been found. There is some experimental evidence for the existence of a threshold velocity and the majority of experimental points lie within the limits for a wedge shaped jet, i.e. between the shock detachment locus and the plane-ended case. For harder materials, surface slope is reduced and there is a certain probability of pitting

occurring below the threshold velocity but this is likely to be a statistical effect induced by random variations in microjet velocity and wedge angle.

The authors gratefully acknowledge the financial support of the Procurement Executive, Ministry of Defence.

REFERENCES

BOWDEN, F. P. & FIELD, J. E. 1964 The brittle fracture of solids by liquid impact, by solid impact and by shock. *Proc. R. Soc. Lond* A **282**, 331–352.

BRUNTON, J. H. & ROCHESTER, M. C. 1979 Erosion of solid surfaces by the impact of liquid drops. In *Treatise on Materials Science and Technology Erosion* (ed. C. M. Preece), vol. 16. Academic.

FIELD, J. E., LESSER, M. B. & DAVIES, P. N. H. 1979 Theoretical and experimental studies of two dimensional impact. *Proc. Fifth Intl Conf. on Erosion by Liquid and Solid Impact, Cambridge, Paper no.* 2.

FIELD, J. E., LESSER, M. B. & DEAR, J. P. 1985 Studies of two-dimensional liquid-wedge impact and their relevance to liquid drop impact problems. *Proc. R. Soc. Lond.* A **401**, 225–249.

GLENN, L. A. 1974 On the dynamics of hypervelocity liquid jet impact on a flat rigid surface. *Z. angew. Math. Phys.* **25**, 383–398.

GRANT, M. McD. 1984 The prediction of cavitation erosion rates. Ph.D. thesis, The City University, London.

HEYMANN, F. J. 1969 High speed impact between a liquid drop and a solid surface. *J. Appl. Phys.* **40**, 5113–5122.

JAUOL, B. 1964 Etude de la plasticité et application aux metaux. Dunod, Paris. Reported in *The Plastic Deformation of Metals* (R. W. K. Honeycombe). Edward Arnold.

KIMOTO, H., TSUDA, Y. & HIROSE, T. 1983 A modelling study of the cavitation microjet. *Proc. I. Mech. E. Conf. on Cavitation, Edinburgh*, pp. 57–62.

LAUTERBORN, W. 1979 Liquid jets from cavitation bubble collapse. *Proc. Fifth Intl Conf. on Erosion by Liquid and Solid Impact, Cambridge, Paper no.* 58.

LESSER, M. B. 1981 Analytic solutions of liquid-impact problems. *Proc. R. Soc. Lond.* A **377**, 289–308.

LESSER, M. B. & FIELD, J. E. 1983 The impact of compressible liquids. *Ann. Rev. Fluid Mech.* **15**, 97–122.

LUSH, P. A. 1979 Surface deformation produced by a cavitating flow. *Proc. Fifth Intl Conf. on Erosion by Liquid and Solid Impact, Cambridge, Paper no.* 61.

LUSH, P. A. 1983 Impact of a liquid mass on a perfectly plastic solid. *J. Fluid Mech.* **135**, 373–387.

LUSH, P. A., WOOD, R. J. K. & CARPANINI, L. J. 1983 Pitting in soft aluminium produced by spark-induced cavitation bubbles. *Proc. Sixth Intl Conf. on Erosion by Liquid and Solid Impact, Cambridge, Paper no.* 5.

PEDERSON, T. F., PEDERSON, S. & HANSSON, I. 1983 Subsurface deformation studies of cavitation eroded FCC materials. *Proc. Sixth Intl Conf. on Erosion by Liquid and Solid Impact, Cambridge, Paper no.* 4.

PENNY, W. A. 1981 The design of a 0.5 MN rotary forging machine and experimental rotary forging. Ph.D. thesis, The City University, London.

PLESSET, M. S. & CHAPMAN, R. B. 1971 Collapse of an initially spherical vapour cavity in the neighbourhood of a solid boundary. *J. Fluid Mech.* **47**, 283–290.

RADISH, D. I. 1984 The investigation of the effects of spark induced cavitation bubbles on a selection of aluminium alloys. Final Year project, Dept. of Mech. Engng, The City University, London.

ROCHESTER, M. C. & BRUNTON, J. H. 1979 Pressure distribution during drop impact. *Proc. Fifth Intl Conf. on Erosion by Liquid and Solid Impact, Cambridge, Paper no.* 6.

TABOR, D. 1951 *The Hardness of Metals.* Oxford University Press.